



HAL
open science

Characteristics and sources of black carbon aerosol in a mega-city in the western Yangtze River Delta, China

Jun Li, Lei Jiang, Cheng Chen, Dantong Liu, Songshan Du, Yunjiang Zhang, Yifan Yang, Lili Tang

► **To cite this version:**

Jun Li, Lei Jiang, Cheng Chen, Dantong Liu, Songshan Du, et al.. Characteristics and sources of black carbon aerosol in a mega-city in the western Yangtze River Delta, China. *Atmosphere*, 2020, 11 (4), 10.3390/atmos11040315. hal-02677095

HAL Id: hal-02677095

<https://hal.science/hal-02677095>

Submitted on 8 Jun 2020

HAL is a multi-disciplinary open access archive for the deposit and dissemination of scientific research documents, whether they are published or not. The documents may come from teaching and research institutions in France or abroad, or from public or private research centers.

L'archive ouverte pluridisciplinaire **HAL**, est destinée au dépôt et à la diffusion de documents scientifiques de niveau recherche, publiés ou non, émanant des établissements d'enseignement et de recherche français ou étrangers, des laboratoires publics ou privés.

Article

Characteristics and Sources of Black Carbon Aerosol in a Mega-City in the Western Yangtze River Delta, China

Jun Li ^{1,2,3}, Lei Jiang ^{3,4}, Cheng Chen ^{2,*}, Dantong Liu ⁵, Songshan Du ², Yunjiang Zhang ⁶, Yifan Yang ³ and Lili Tang ³

¹ Lianyungang Environmental Monitoring Center of Jiangsu Province, Lianyungang 222001, China; lygjc3s@126.com

² Jiangsu Environmental Monitoring Center, Nanjing 210036, China; dusongshan01@gmail.com

³ Jiangsu Collaborative Innovation Center of Atmospheric Environment and Equipment Technology, Nanjing University of Information Science & Technology, Nanjing 210044, China; jianglei1836209@163.com (L.J.); yifan_yang424@163.com (Y.Y.); lily3258@163.com (L.T.)

⁴ ED129, Sorbonne University, UPMC Univ Paris 06, 750050 Paris, France

⁵ Department of Atmospheric Science, School of Earth Sciences, Zhejiang University, Hangzhou 310027, China; dantongliu@zju.edu.cn

⁶ Laboratoire des Sciences du Climat et l'Environnement, CNRS-CEA-UVSQ, 91191 Gif sur Yvette, France; yunjiang.zhang@lsce.ipsl.fr

* Correspondence: cc@jshb.gov.cn; Tel.: +86-25-8657-5233

Received: 20 February 2020; Accepted: 19 March 2020; Published: 25 March 2020



Abstract: A single particle soot photometer (SP2) was deployed in urban Nanjing, located in the Yangtze River Delta (China), to investigate the mixing state and sources of ambient refractory black carbon (rBC) from 26 January to 25 February 2014, along with an in-situ measurement of submicron aerosol chemical species by an aerodyne aerosol chemical speciation monitor (ACSM). The results showed that anthropogenic activities associated with firework emissions can be a significant source for rBC-containing particles during the period of the Chinese New Year, resulting from the evident peaks of rBC at midnight. During the residual periods, namely regular day (RD), the diurnal cycles of rBC presented two typical peaks that can be attributed to a synergistic influence of local traffic emissions and boundary layer changes throughout a day. Three coating factors, including organics, sulfate, and nitrate (-rich), were resolved using a positive matrix factorization (PMF) approach to explain the potential contribution of non-rBC coatings (i.e., organics, sulfate, and nitrate) to the coating thickness of rBC-containing particles. As the results show, organic aerosols (OAs) might be a major contributor to the coating thickness of rBC-coating particles during the whole period. The relative coating thickness (a ratio between coated particle size to BC core) exhibited a positive relationship with sulfate, indicative of the favorable coating factor during the episode caused by firework emissions. Source apportionment of rBC was performed via a multiple linear regression between the total rBC mass and each ACSM-PMF factor (rBC-ACSM-PMF). On average, biomass burning emissions accounted for 43%, being the largest contributor during the RD period, whereas local traffic emissions played a major role during the new year time.

Keywords: black carbon; mixing state; sources; firework emissions; winter; Yangtze River Delta

1. Introduction

Atmospheric black carbon (BC) aerosol plays a significant role in climate warming effects by absorbing solar radiation [1–3], the source of which is mainly emitted from incomplete combustion

processes of fossil fuel or biomass burning [2]. Since the size distributions of BC particles are mostly in the range of 0.01 to 1 μm , they can enter the blood stream through the respiratory system, deteriorating the health condition of human beings [4]. High BC concentrations have been frequently observed in eastern China, which has been suffering from serious air pollution issues [5]. Recently, it has also been realized that haze pollutions can be induced by high concentrations of BC aerosols over eastern China [5]. However, the physical and chemical properties and sources of BC-containing particles remain poorly understood in eastern China, which is essential to be further investigated.

The surface structure of fresh BC particles is loose and porous, which provides a place for the adsorption of coating components. The physical and chemical properties of the BC-containing particle can be changed via accumulating coatings of non-refractory chemical species. The mixture of BC and coating components in the forms of internal mixing can lead to the particle absorption efficiency enhancement, which depends on the aging degree of particles in the atmosphere [6–9]. Previous aircraft measurements suggested that the coatings enhance light absorption of BC column by at least 30% in the free troposphere [10]. Besides, the absorption coefficient of refractory black carbon (rBC)-containing particles shows regionally-specific characterizations, which had different effects but all could contribute importantly to atmospheric stabilization and the boundary layer variation [11,12]. The light absorption capacity of BC varies slightly in the first stage and the spherical particles continue to increase with a large absorption enhancement, up to 2.4 times compared to the initial absorption capacity [12]. Fresh BC particles are mainly hydrophobic when emitted, but it can become hygroscopic after atmospheric aging [13]. Liu et al. [14] found that the hygroscopicity of BC particles can be increased when they are coated by secondary inorganic aerosols, especially ammonium nitrate. However, quantitative analysis on the mixing state and sources of rBC particles in China, especially in polluted regions (e.g., the Yangtze River Delta), remain unclear. Understanding the mixing state of ambient BC is therefore particularly important to evaluate their lifetime and environmental impacts.

Several instruments have been successfully applied for quantification on BC mass concentration, e.g., organic carbon/elemental carbon (OC/EC) analyzer and Aethalometer, but they are not able to provide the information on single BC particles. Recently, a useful instrument, the single particle soot photometer (SP2), was developed to characterize the physical properties of refractory black carbon (rBC) particles [15,16]. The SP2 can measure the mass, number concentrations, and size distribution of rBC with high time resolution. The mixing state of individual rBC particles measured by the SP2 can then be calculated using a concentric core-shell configuration, which has been described in detail by Taylor et al. [17]. In this study, a combination of the SP2 and an Aerodyne Aerosol Chemical Speciation Monitor (ACSM) was employed to investigate the characterization of the mixing state and sources of rBC in wintertime in urban Nanjing, a megacity in the Yangtze River Delta (YRD). Potential coatings of non-refractory chemical species on rBC-containing particles were explored. A new insight into the impact of firework emissions on mixing state of rBC was discussed.

2. Experiment

2.1. Sampling Site

The YRD is one of the most developed economic regions in China and plays an important role in contributing to the nation's continuous economic growth. The sampling site (32°03' N, 118°46' E) was located in the urban area of Nanjing, one of the largest cities in the YRD (Figure 1).

The measurements took place during the wintertime from 26 January to 25 February 2014. All instruments were conducted on the roof of a six-story building in Jiangsu Provincial Environment Monitoring Center, approximately 18 m vertically from the ground. This sampling site can be an influence of multiple sources, e.g., local emissions and regional transports, which is a typical residential, commercial, and business area of urban environments. In addition, short-term impacts of firework emissions on the local air quality could be associated with firework events over the region of the sampling site during the Chinese Lunar New Year.

2.2. Instrument Description

2.2.1. The Single Particle Soot Photometer

In this study, SP2 was used to measure single rBC-containing particles. A detailed description of the SP2 can be found in previous studies [16,18,19]. Briefly, SP2 is based on the absorption of BC in the near-infrared band. Particles are drawn through an intra-cavity neodymium: yttrium-aluminum-garnet (Nd:YAG) laser ($\lambda = 1064$ nm) and heated one by one. The soot particles can be heated to their vaporization temperature and they emit an incandescent signal, while other particles just scattering light can only emit a scattering signal. All the signals are captured by four different light detectors, while the intensity of the incandescent light is proportional to the mass of rBC regardless of particle coatings or morphology [14]. Refractory components have high enough boiling point temperatures that they emit an incandescent signal as they vaporize. Hence, the amount of rBC is determined by the peak intensity of the incandescent signal [20]. The broadband detector for individual rBC particle mass detection ranges from 0.3–67 fg and corresponding rBC equivalent volume diameter from 67–305 nm, the narrowband detector for individual rBC particle ranges from 1.6–130 fg and the corresponding rBC equivalent volume diameter from 82–550 nm, covering the vast majority of rBC particles in the atmosphere [19,21]. The sampling flow rate was set at 60 mL/min.

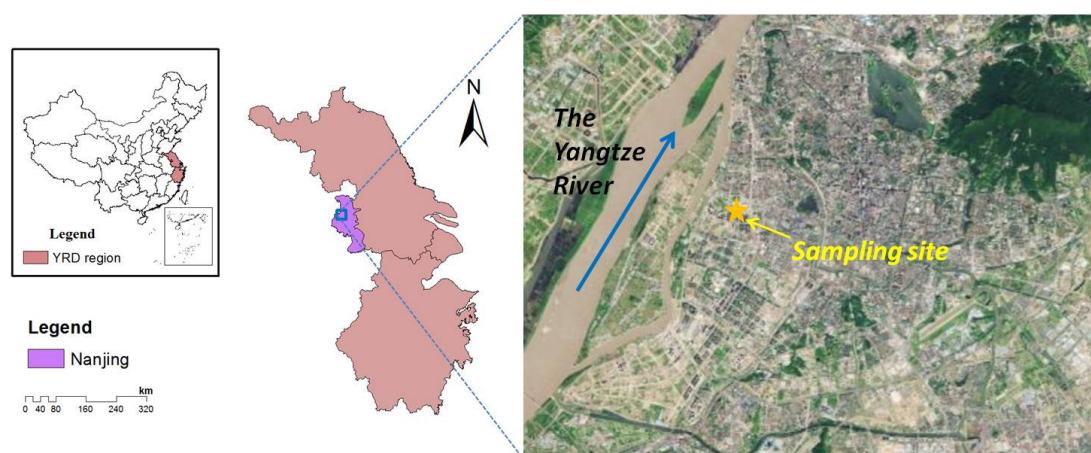


Figure 1. Sampling site of Nanjing.

When rBC are coated by other chemical components, they can transfer the heat to the surface, and some time is taken for coatings to evaporate before incandescence can occur. The aging degree of rBC was then inferred from the time delay between the peak of the scattering and incandescent signal [10]. The scattering signal of particles is discussed based on the assumption that particles are spherical and uniform. The scattering process of the electromagnetic wave is obtained by using the electromagnetic field equation. The measuring method for the coating thickness assumes that the rBC is a spherical structure and the pure BC is coated by non-refractory components. Mostly ambient rBC particles contain non-refractory materials, so coated rBC sizes (D_p) and pure rBC sizes, also termed rBC core size (D_c), were input to the Mie calculations. Previous studies have defined the most appropriate core refractive index and coating refractive index to be $2.26 - 1.26i$ and $1.5 + 0i$ respectively [17,22–24], the parameters of which was used in Mie model calculation in this study. The relative outer shell thickness can be defined as D_p/D_c . The imaginary part of the refractive index of 1.26 that we use is specifically for the SP2 configuration at the laser wavelength of 1064 nm, which has been previously tested using pure-BC of denuded diesel soot, and this value will give a $D_p/D_c = 1$ for such nearly-pure BC at 1064 nm. The SP2 can measure tens of thousands of particles per minute and the data that we used in this study was hourly average data. Therefore, the error caused by the size of single particles is largely offset, which basically reflects the relative aging process of

rBC in this period. The incandescence signal was calibrated using Aquadag® black carbon particles (Aqueous Deflocculated Acheson Graphite, manufactured by Acheson Inc., Port Huron, MI USA). The Aquadag® black carbon particles were selected by mobility diameter using a differential mobility analyzer (DMA). The DMA voltage was adjusted to obtain data of about ten thousand BC particles in the mobility diameter range of ~80 to ~500 nm to establish a functional relationship between the peak height of the wide-channel optical signal and the particle mass.

2.2.2. Other Instrument and Data

The non-refractory submicron aerosol species, including organic aerosol (OA), sulfate, nitrate, ammonium, and chloride were measured by the ACSM, which operated at a time resolution of ~15 min with a scan from m/z 10 to 150 atomic mass unit (amu) at a rate of 500 ms amu⁻¹ [25,26]. A detailed description for the operational principles of the instrument and data analysis can be found elsewhere [27,28]. Briefly, the same aerosol sampling, vaporization, and ionization modules are applied in the ACSM system as the Aerodyne Aerosol Mass Spectrometer [29], but, the ACSM cannot provide size information of the measured aerosol chemical composition [28]. Source apportionment of OA was performed using a positive matrix factorization (PMF), which can be found in Supplementary Text S1. Briefly, the PMF results were examined through an Igor Pro-based PMF Evaluation Tool [30]. The detailed description of PMF can be found elsewhere [31]. A monitoring of aerosols and gases (MARGA, model ADI 2080 Applikon Analytical B. V. Corp., Herisau, The Netherlands) was also deployed to measure the mass concentrations of a major water-soluble inorganic ion (potassium ion, K⁺) in PM_{2.5}. All collocated gaseous species, including NO-NO₂-NO_x, O₃, SO₂ and CO, were measured with gas analyzers (Thermo Scientific, Singapore).

3. Results and Discussions

3.1. rBC Mass Loadings

3.1.1. Time Series of rBC Mass Concentration

Figure 2 shows the time series of hourly-averaged wind speed (WS), wind direction (WD), temperature, relative humidity (RH), precipitation, D_p/D_c , and rBC mass concentrations obtained during the whole period. The average WS was 3.31 m/s with a range of 0.1–7.8 m/s. The RH and temperature varied between 33% to 99% and –5.4 to 20.4 °C, with an average of 78% and 4.9 °C, respectively. Low intensity rainfall occurred four times over the whole period. We attempted to divide the total period into two periods: A Spring Festival period (SF, also termed as Chinese New Year) and residual days (Regular Days, RD).

The rBC mass concentrations varied from 0.12 to 11.72 µg/m³ during the whole period, with an average of 3.02 ± 2.12 (mean $\pm 1\sigma$) µg/m³. On average, it was observed that the mass concentration of rBC during the SF (3.65 ± 2.95 µg/m³) was found to be 0.85 µg/m³ higher than that during the RD (2.80 ± 1.68 µg/m³). On average, the D_p/D_c was similar during the periods between the SF (1.34) and the RD (1.36), which is consistent with the values observed in other cities in the presence of strong traffic emissions [23,32]. This might suggest that fresh rBC-containing particles, rather than more aged ones, could dominate the amount of total rBC particles during the entire study. Meteorological factors also played an important role in rBC mass concentration trends. As an illustration, Figure 2d shows a high mass loading around 27 January, which is most likely due to low WS and unstable WD. Since static weather conditions are not conducive to the spread of locally produced pollutants, this therefore could have accounted for the high concentration loadings of rBC.

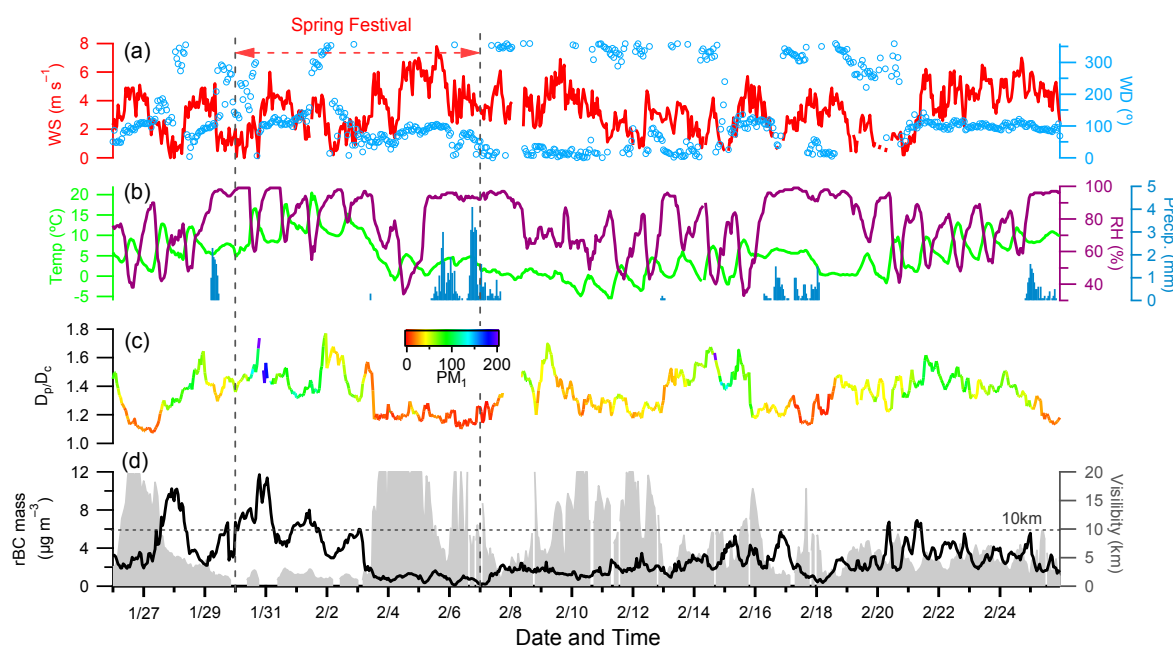


Figure 2. Time series of hourly-average (a) wind speed, wind direction, (b) temperature, relative humidity, precipitation, (c) relative coating thickness coated/uncoated diameter (D_p/D_c), and PM_{10} , (d) visibility and mass concentrations of refractory BC (rBC).

3.1.2. Diurnal Variation of rBC Mass Concentration

Figure 3 depicts the diurnal variations of the rBC mass concentration over the entire period. All time references are given in local standard time (LST). During the RD period, rBC presented two obvious peaks at early morning (around 08:00 LST) and evening (around 19:00 LST) rush hours, which are likely associated with rush hours and could be influenced by variations of planetary boundary layer height [23,33,34]. The height of the boundary layer rises with ascending of the solar radiations in the afternoon, therefore creating meteorological conditions that were conducive for the dispersion of pollutants. This can be one of the important factors affecting the concentrations of rBC particles in ambient air. The mass concentration of rBC presented insignificant diurnal variations during the SF period. This can be partly explained by a reduction in BC emissions from the regular transportation sector during the SF vacation period. During the vacation period, residents are not required to go to work within a fixed timeline, therefore the change in trend did not show the usual morning and evening peaks.

3.2. rBC Mixing State

3.2.1. Diurnal Variation and Quantification of Each Components

The diurnal variation patterns of D_p/D_c are shown in Figure 4. The average D_p/D_c was 1.34 (SF) and 1.36 (RD), respectively. Diurnal cycles on RD had higher D_p/D_c values in the early morning and afternoon, as well as two lower values with one in the morning rush hours (06:00–08:00) and the other in the evening. This means that the coating thickness of rBC was relatively high in the early morning and afternoon, with fresh particles near the source emissions at the rush hours. The atmospheric boundary layer was relatively low during the night, subsequently making the diffusion of pollutants difficult and led to coatings on rBC. D_p/D_c kept relatively stable with a weak decrease during daytime in the SF. High RH in the morning enhanced the component's hygroscopic properties coated on the rBC [14], and strong solar radiation also accelerated the photochemical reaction during the daylight.

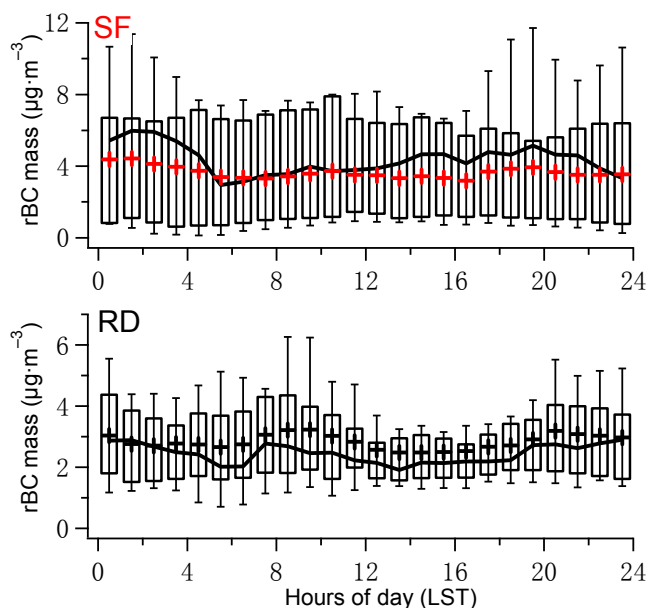


Figure 3. Mean diurnal variation patterns of rBC concentrations for spring festival and regular day (The upper and lower edges of the box denote the 25% and 75% percentiles, respectively. The lines in the middle of the box and cross markers indicate the median and average values respectively, with error bars explaining the 10% and 90% percentiles.).

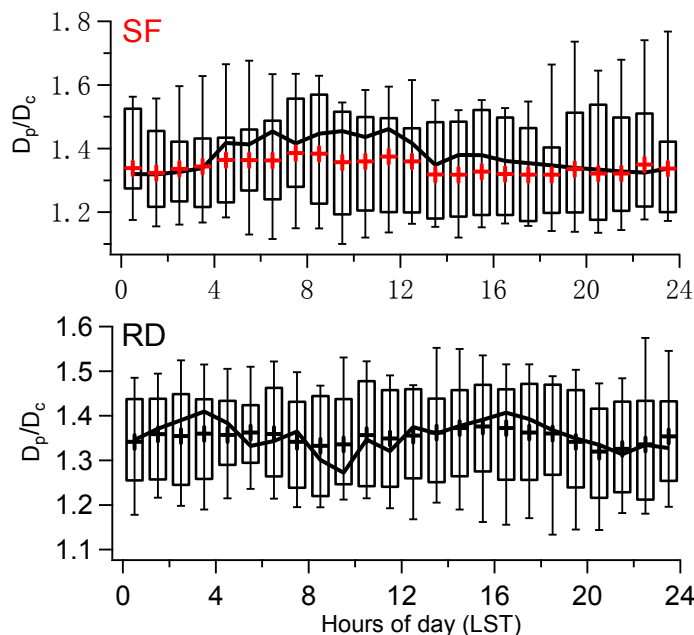


Figure 4. Mean diurnal variation patterns of D_p/D_c for spring festival and regular day (The upper and lower edges of the box denote the 25% and 75% percentiles, respectively. The lines in the middle of the box and cross markers indicate the median and average values respectively, with error bars explaining the 10% and 90% percentiles.).

In addition, an EPA3.0 PMF model was used to evaluate the contributions by sulfate, nitrate, and organics on rBC coating thickness [35–39]. This method was based on assuming that all the rBC can be coated by other components measured by the ACSM. However, there could be some pure rBC particles that were not coated by any aerosol chemical coating in the atmosphere, those parts of which cannot be well explained due to the limitation of the instruments. The mass ratio between sulfate, organics, and nitrate to that of rBC [36] and the relative coating thickness (f_{BC}) ($f_{BC} = (D_p - D_c)/D_c$)

are the data input to the PMF model. The values of $(\text{OA})/(\text{rBC})$, $(\text{sulfate})/(\text{rBC})$, $(\text{nitrate})/(\text{rBC})$ and f_{BC} predicted by the PMF model agree well with the observed values ($R^2 = 0.84, 0.99, 0.99, 0.87$ during the SF and $R^2 = 0.82, 0.99, 0.99, 0.82$ during the RD, respectively). The data validation and a detail description of the fitting results are given in the Supplementary Materials, Figure S1, Text S2, and Table S1.

Factor 1 explained high loadings of $(\text{SO}_4)/(\text{rBC})$, indicating that sulfate could dominate the coating materials. Factor 2 showed that $(\text{OA})/(\text{rBC})$ occupy a major proportion, meaning that organics could be the main component among those coatings. Factor 2 is likely the most important one among the three factors, because Factor 2 was the main contributor for the f_{BC} during both SF and RD. Factor 3 was mainly composed of $(\text{NO}_3)/(\text{rBC})$, suggesting that nitrate could be the major contributor to the rBC coating thickness. Therefore, those factors could be defined as sulfate-related (Factor 1), OA-related (Factor 2), and nitrate-related (Factor 3) coating sources, respectively [35,37,39].

As shown in Figure 5, sulfate-related and OA-related factors have contributed around 90% of f_{BC} over the SF. This indicates that both sulfate and organics constituted to the principal chemical coatings of rBC-containing. Factor 3 also showed high loadings of nitrate, but a very low level of f_{BC} , which means that nitrate-related components might not be a main component of the rBC's coatings. During the RD, Factors 2 and 3 contributed predominantly to f_{BC} , signifying that nitrates and organics directly constituted the components of the coatings, whereas sulfate might not represent an important part of the coatings. While comparing the two sets of results, it can be seen that Factor 2 was the most important part of the results in both periods, and contributed more than half of the coating components, while Factor 1 and Factor 3 showed different effects in the two time regimes.

3.2.2. Quantification of Firework Event

Firework ignition has been found to emit large amounts of potassium ions (K^+), which is a well-established tracer for a firework event (FE) [40,41]. As shown in Figure 6, the entire process took place from 16:00 on 30 January to 3:00 of the next morning, as indicated by the blue arrow. Two significant increments of K^+ concentrations were observed on the first day of the Lunar New Year, one at 19:00 and another at 00:00 on 31 January, which are defined as FE1 and FE2, respectively. Coincidentally, a rapid change in wind direction and firework burning occurred simultaneously during the FE1. As shown in Figure 6d, secondary aerosol species (e.g., SO_4 , and NO_3) substantially increased which corresponded to the change of K^+ . Apparently, the primary species (e.g., SO_2 , CO, and NO) also showed obvious changes. Section 3.2.1 has illustrated that Factors 1, 2, and 3 were the sulfate-related coatings, OA-related coatings, and nitrate-related coatings, respectively. Generally, the contribution of each component to the rBC coating thickness showed that the contributions of sulfate and nitrate increased when that of OA decreased. Comparing between Figure 6d and e, it was found that Factors 1 and 3 presented a similar change in trends with respect to sulfate and nitrate, but Factor 2 was not matched well with the oxygenated organic aerosol (OOA), where OOA can be considered as a surrogate of secondary OA [42,43]. Thus, it can be explained that Factor 2 contains a large amount of primary organic matter for both FE1 and FE2. After the FE1, the pollutants had spread due to the rise in WS. The proportion of Factor 2 decreased with increasing D_p/D_c and had a minimum value when Factor 2 was at the peak value. This phenomenon further supports the assertion that Factor 2 was mainly composed of primary organic aerosols (POA) at the FE. The thickest outer shell thickness of rBC was observed at the same time as the peak K^+ concentration of both FE1 and FE2, which means that the coating process for rBC was mostly influenced by the transformation of particulate matter from local pollutants during the whole course of the FE. Figure 6e also shows that the coating thickness of rBC was most closely related to Factor 1, indicating that sulfate might be the main non-refractory coating material.

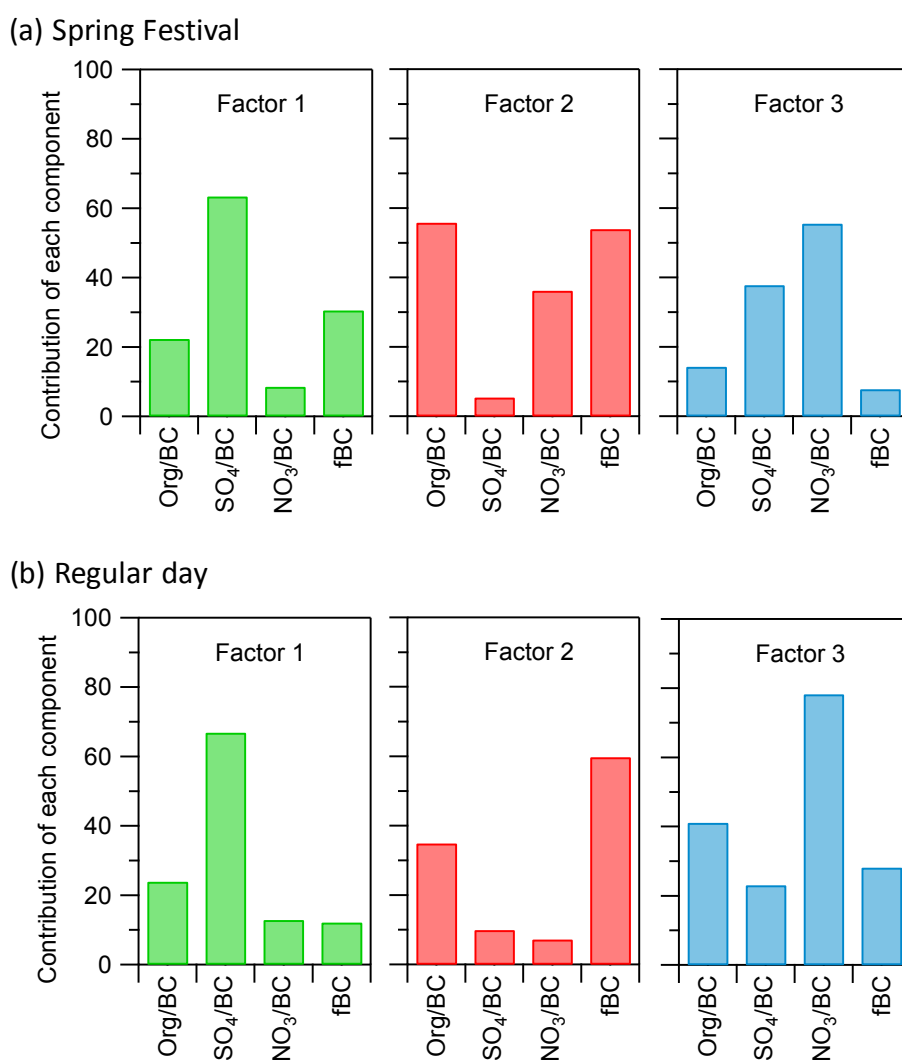


Figure 5. Contribution of different components for (a) spring festival and (b) regular day.

3.3. rBC Source Attribution by SP2 and ACSM

Using a multiple linear regression analysis to identify sources of rBC, the ACSM-PMF OA factors and rBC were used as the inputs of the calculations. Supplementary Figure S2 presents the mass spectra of PMF OA factors, including hydrocarbon-like OA (HOA), biomass burning OA (BBOA), and oxygenated OA (OOA). The HOA spectrum, characterized by $C_nH_{2n-1}^+$ and $C_nH_{2n+1}^+$, is consistent with those resolved at urban sampling sites [14,34,41,44]. In fact, the HOA factor in the urban environment has been well known to be mainly generated from traffic emissions [14,34,41,44]. The mass spectrum of BBOA was characterized by evident signals at m/z 60 and m/z 73, two typical markers indicative of biomass burning. The mass spectrum of OOA, a surrogate of secondary organic aerosol (SOA) with regional characteristics [43,44], was mainly dominated by m/z 44. Negligible contribution of m/z 60 and hydrocarbon ion series to the OOA spectrum could further support a good PMF model performance to apportion primary (i.e., HOA and BBOA) and secondary (i.e., OOA) OA factors in the present study. Therefore, local vehicular emissions can be represented by HOA, while BBOA can represent rBC coming from biomass burning [25]. OOA could represent aged or oxidized rBC-containing particles coming from regional transport [33]. Thus, the formula of the mass of rBC (mBC) can be described as follows:

$$mBC_{\text{Total}} = a (\text{HOA}) + b (\text{BBOA}) + c (\text{OOA})$$

To better estimate the relationship between the rBC_{measured} and rBC_{modeled}, we first removed all the instantaneous extremes of both OA and rBC. As shown in Figure 7, a good correlation between rBC_{measured} and rBC_{modeled} was observed with a linear regression, $r^2 = 0.79$. Note that this method is feasible in practical application [44].

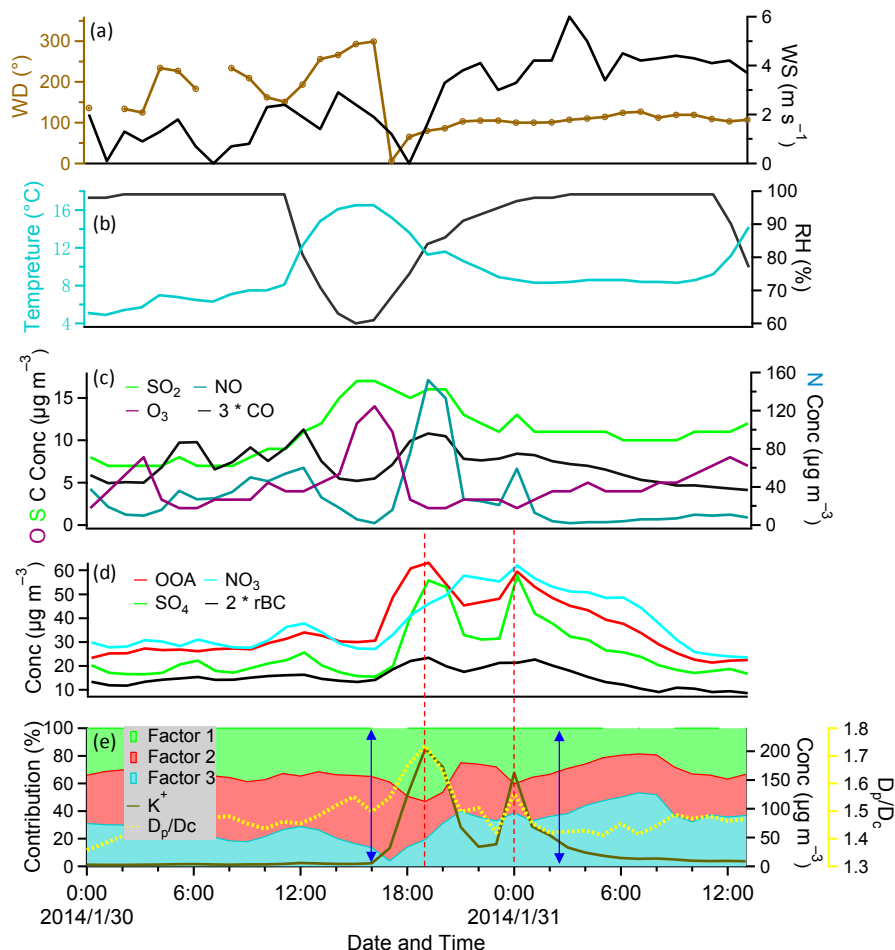


Figure 6. Time series of hourly average (a) wind speed, wind direction, (b) temperature, relative humidity, (c) mass concentrations of sulfur dioxide, nitric oxide, ozone, carbon oxide, (d) mass concentrations of oxygenated organic aerosol, nitrate, sulfate, rBC, (e) D_p/D_c , contribution of different components and potassium ion mass concentrations. Note that concentrations of CO (3*CO) and rBC (2*rBC) have been multiplied by the factors of 3 and 2, respectively, to better visualize their trends.

The regression results, as shown in Figure 8, indicate the good performance of both rBC_{measured} and rBC_{modeled} during most of the time. The regression coefficients (a), (b) and (c) are shown in Table 1. The coefficient of traffic emission which influenced Factor (a) during SF ($a = 0.949$) was higher than that observed during the RD ($a = 0.408$). Local vehicular emissions accounted for 45% and 32% of the total rBC during the SF and RD, respectively. The Factor (a) continuously followed a downward trend away from urban areas [23], but the instruments were set at the same observation site throughout the whole observation period. This is because vehicular emissions were concentrated in the morning and evening rush hours during the RD, but the distribution of vehicular emissions were more uniform during the SF. In view of this, Factor (a) displayed a higher value based on the statistical evidence, because the industrial production process was brought to a halt during the entire vacation period. This could have accounted for the reason behind traffic emission constituting the major source of rBC during the SF. The coefficient of regional transport influencing Factor (c) was found to be in very small numbers during both SF and RD, but due to the high concentrations of OOA during the whole

time, regional transport contributed around 25% to all rBC in both periods. Figure 8b also shows that the model always underestimates rBC mass concentration when D_p/D_c is low and frequently over-estimates it when the outer shell thickness of rBC is relatively thicker. This might be due to the fact that we did not take into account some fresh emission sources of rBC in the model, and then overestimated the influence of regional transport. The OOA may contain some local aging secondary OA that cannot be classified as part of the regional emission sources of rBC. This also indicates that more work needs to be done in further research.

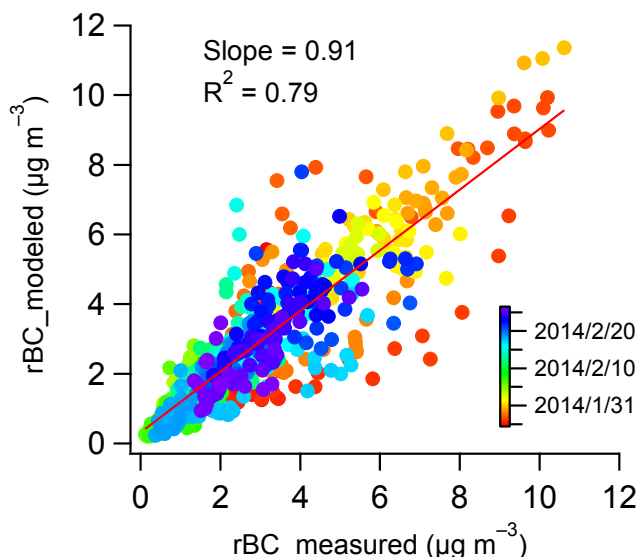


Figure 7. Linear fit between measured and modeled rBC.

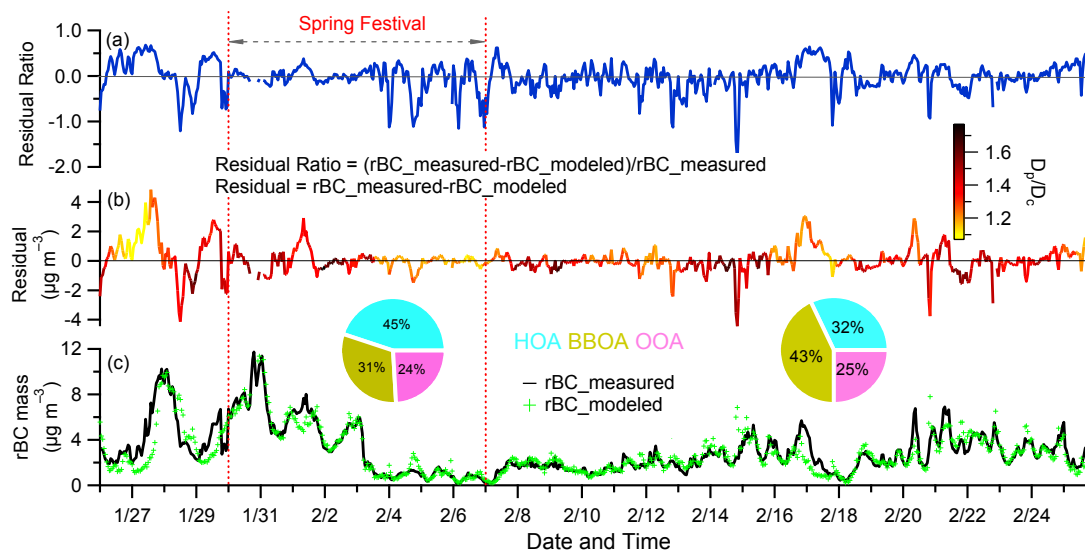


Figure 8. Modeled rBC mass by tri-linear regression compared with the measurements: (a) time series of the ratio of the residual to the measured rBC, (b) time series of the residual of the fit to the measured rBC, (c) the variations of the fitting residuals and the average contribution of different components to rBC.

Table 1. The tri-linear regression results for the rBC-ACSM-PMF attribution.

| Period | a | b | c | r ² |
|----------------------|---------------|---------------|---------------|----------------|
| Spring Festival (SF) | 0.949 ± 0.061 | 0.224 ± 0.027 | 0.053 ± 0.010 | 0.98 |
| Regular Days (RD) | 0.408 ± 0.036 | 0.328 ± 0.017 | 0.057 ± 0.006 | 0.90 |

4. Conclusions

Characterization of the mixing state and sources of rBC aerosols in Nanjing's urban areas, the YRD region of China, was investigated using the SP2 during the wintertime with special emphasis on the SF. The experiment was conducted from 26 January to 25 February 2014. The results showed that the mean rBC mass concentration was found to be around $3.65 \pm 2.95 \mu\text{g}/\text{m}^3$ and $2.80 \pm 1.68 \mu\text{g}/\text{m}^3$ during SF and RD, respectively. The daily variation of the rBC mass had two peak values on RD, which was mostly influenced by meteorological factors and human activities but showed obvious differences during SF. The rBC mass had a remarkable increase shortly after midnight due to many fireworks' ignition, which is a typical "Chinese characteristic". A PMF model indicated that organics played a major role in rBC's coatings in the two periods, but sulfate constituted another main component contributing to the coating during SF, whereas nitrate contributed more during RD. The coating thickness of rBC was higher before sunrise in the early morning and early afternoon during SF and lower in the morning and evening during RD, and the outer shell thickness of rBC was also thicker at the same time. The shell thickness of rBC was heavily influenced by local lighting of fireworks, which particularly increased with the increased sulfate. The rBC-ACSM-PMF showed that local vehicular emissions made up 45% and 32% of the total rBC during the SF and RD, suggesting that vehicular traffic emissions were the dominating source of rBC in the period of SF and the regression coefficient (a) is higher than for RD. However, the contribution of biomass combustion was the exact opposite of local vehicular emissions, and rBC by regional transport was similar during both periods.

Supplementary Materials: The following are available online at <http://www.mdpi.com/2073-4433/11/4/315/s1>, Text S1: PMF method description; Figure S1: Liner fit between NR-PM1 (organics, sulfate, nitrate, ammonium and chloride) which were measured by ACSM and mass concentration of PM_{2.5} from Jiangsu meteorological station network; Table S1: Contribution of each component during Spring Festival (SF) and Regular Days (RD); Text S2: The meaning of average fraction of measured signal by each factor; Figure S2: Mass spectra of hydrocarbon-like OA (HOA), oxygenated OA (OOA) and biomass burning OA (BBOA) factors resolved by ACSM-PMF analysis.

Author Contributions: Conceptualization, J.L.; data curation, D.L., Y.Z., and Y.Y.; formal analysis, L.J. and S.D.; funding acquisition, J.L. and C.C.; investigation, L.T.; methodology, D.L. and Y.Z.; project administration, J.L. and L.T.; resources, S.D.; software, D.L.; supervision, C.C.; validation, S.D.; writing—original draft, J.L. and L.J.; writing—review and editing, L.T. All authors have read and agreed to the published version of the manuscript.

Funding: This research was funded by the Lianyungang Environmental Monitoring Center of Jiangsu Province project "Research and demonstration Application of PM_{2.5}, Ozone, and its precursors Monitoring system, quality Control and quality Assurance system".

Acknowledgments: We would like to thank Min Hu from Peking University and Yun Fei Wu from the Institute of Atmospheric Physics for their constructive criticism on the manuscript.

Conflicts of Interest: The authors declare no conflict of interest.

References

1. Andreae, M.O. The dark side of aerosols. *Nature* **2001**, *409*, 671–672. [[CrossRef](#)]
2. Bond, T.C.; Doherty, S.J.; Fahey, D.W.; Forster, P.M.; Berntsen, T.; DeAngelo, B.J.; Flanner, M.G.; Ghan, S.; Kärcher, B.; Koch, D.; et al. Bounding the role of black carbon in the climate system: A scientific assessment. *J. Geophys. Res. Atmos.* **2013**, *118*, 5380–5552. [[CrossRef](#)]
3. Raatikainen, T.; Brus, D.; Hyvärinen, A.P.; Svensson, J.; Asmi, E.; Lihavainen, H. Black carbon concentrations and mixing state in the Finnish Arctic. *Atmos. Chem. Phys.* **2015**, *15*, 10057–10070. [[CrossRef](#)]
4. Jacobson, M.Z. Short-term effects of controlling fossil-fuel soot, biofuel soot and gases, and methane on climate, Arctic ice, and air pollution health. *J. Geophys. Res.* **2010**, *115*, D14209. [[CrossRef](#)]
5. Ding, A.J.; Huang, X.; Nie, N.; Sun, J.; Kerminen, V.-M.; Petaja, T.; Su, H.; Cheng, Y.F.; Yang, X.-Q.; Wang, M.H.; et al. Enhanced haze pollution by black carbon in megacities in China. *Geophys. Res. Lett.* **2016**, *43*, 2873–2879. [[CrossRef](#)]
6. Zhang, R.; Khalizov, A.F.; Pagels, J.; Zhang, D.; Xue, H.; McMurry, P.H. Variability in morphology, hygroscopicity, and optical properties of soot aerosols during atmospheric processing. *Proc. Natl. Acad. Sci. USA* **2008**, *105*, 10291–10296. [[CrossRef](#)]

7. Cappa, C.D.; Onasch, T.B.; Massoli, P.; Worsnop, D.R.; Bates, T.S.; Cross, E.S.; Davidovits, P.; Hakala, J.; Hayden, K.L.; Jobson, B.T.; et al. Radiative absorption enhancements due to the mixing state of atmospheric black carbon. *Science* **2012**, *337*, 1078–1081. [[CrossRef](#)]
8. Lan, Z.J.; Huang, X.F.; Yu, K.Y.; Sun, T.L.; Zeng, L.W.; Hu, M. Light absorption of black carbon aerosol and its enhancement by mixing state in an urban atmosphere in South China. *Atmos. Environ.* **2013**, *69*, 118–123. [[CrossRef](#)]
9. Lee, W.L.; Liou, K.N.; He, C.; Liang, H.-C.; Wang, T.-C.; Li, Q.; Liu, A.; Yue, Q. Impact of absorbing aerosol deposition on snow albedo reduction over the southern Tibetan plateau based on satellite observations. *Theor. Appl. Climatol.* **2016**, *129*, 1373–1382. [[CrossRef](#)]
10. Schwarz, J.P.; Gao, R.S.; Spackman, J.R.; Watts, L.A.; Thomson, D.S.; Fahey, D.W.; Ryerson, T.B.; Peischl, J.; Holloway, J.S.; Trainer, M.; et al. Measurement of the mixing state, mass, and optical size of individual black carbon particles in urban and biomass burning emissions. *Geophys. Res. Lett.* **2008**, *35*, L13810. [[CrossRef](#)]
11. Guo, S.; Hu, M.; Zamora, M.L.; Peng, J.; Shang, D.; Zheng, J.; Du, Z.; Wu, Z.; Shao, M.; Zeng, L.; et al. Elucidating severe urban haze formation in China. *Proc. Natl. Acad. Sci. USA* **2014**, *111*, 17373–17378.
12. Peng, J.F.; Hu, M.; Guo, S.; Du, Z.F.; Zheng, J.; Shang, D.J.; Zamora, M.L.; Zeng, L.; Shao, M.; Wu, Y.-S.; et al. Markedly enhanced absorption and direct radiative forcing of black carbon under polluted urban environments. *Proc. Natl. Acad. Sci. USA* **2016**, *113*, 4266–4271. [[CrossRef](#)]
13. Cheng, Y.F.; Su, H.; Rose, D.; Gunthe, S.S.; Berghof, M.; Wehner, B.; Achtert, P.; Nowak, A.; Takegawa, N.; Kondo, Y.; et al. Size-resolved measurement of the mixing state of soot in the megacity Beijing, China: Diurnal cycle, aging and parameterization. *Atmos. Chem. Phys.* **2012**, *12*, 4477–4491. [[CrossRef](#)]
14. Liu, D.; Allan, J.; Whitehead, J.; Young, D.; Flynn, M.; Coe, H.; McFiggans, G.; Fleming, Z.L.; Bandy, B. Ambient black carbon particle hygroscopic properties controlled by mixing state and composition. *Atmos. Chem. Phys.* **2013**, *13*, 2015–2029. [[CrossRef](#)]
15. Stephens, M.; Turner, N.; Sandberg, J. Particle identification by laser-induced incandescence in a solid-state laser cavity. *Appl. Opt.* **2003**, *42*, 3726–3736. [[CrossRef](#)]
16. Schwarz, J.P.; Gao, R.S.; Fahey, D.W.; Thomson, D.S.; Watts, L.A.; Wilson, J.C.; Reeves, J.M.; Darbeheshti, M.; Baumgardner, D.G.; Kok, G.L.; et al. Single-particle measurements of mid-latitude black carbon and light-scattering aerosols from the boundary layer to the lower stratosphere. *J. Geophys. Res. Atmos.* **2006**, *111*, D16207. [[CrossRef](#)]
17. Taylor, J.W.; Allan, J.D.; Liu, D.; Flynn, M.; Weber, R.; Zhang, X. Assessment of the sensitivity of core/shell parameters derived using the single-particle soot photometer to density and refractive index. *Atmos. Meas. Tech.* **2015**, *8*, 1701–1718. [[CrossRef](#)]
18. Moteki, N.; Kondo, Y. Effects of mixing state on black carbon measurements by laser-induced incandescence. *Aerosol Sci. Technol.* **2007**, *41*, 398–417. [[CrossRef](#)]
19. Liu, D.; Flynn, M.; Gysel, M.; Targino, A.; Crawford, I.; Bower, K.; Choularton, T.; Juranyi, Z.; Steinbacher, M.; Hüglin, C.; et al. Single particle characterization of black carbon aerosols at a tropospheric alpine site in Switzerland. *Atmos. Chem. Phys.* **2010**, *10*, 7389–7407. [[CrossRef](#)]
20. Slowik, J.G.; Cross, E.S.; Han, J.H.; Davidovits, P.; Onasch, T.B.; Jayne, J.T.; Williams, L.R.; Canagaratna, M.R.; Worsnop, D.R.; Chakrabarty, R.-K.; et al. An inter-comparison of instruments measuring black carbon content of soot particles. *Aerosol Sci. Technol.* **2007**, *41*, 295–314. [[CrossRef](#)]
21. Schwarz, J.P.; Spackman, J.R.; Gao, R.S.; Perring, A.E.; Cross, E.; Onasch, T.B.; Ahern, A.; Wrobel, W.; Davidovits, P.; Olfert, J.; et al. The detection efficiency of the single particle soot photometer. *Aerosol Sci. Technol.* **2010**, *44*, 612–628. [[CrossRef](#)]
22. Moteki, N.; Kondo, Y.; Nakamura, S. Method to measure refractive indices of small nonspherical particles: Application to black carbon particles. *J. Aerosol Sci.* **2010**, *41*, 513–521. [[CrossRef](#)]
23. Liu, D.; Allan, J.D.; Young, D.E.; Coe, H.; Beddows, D.; Fleming, Z.L.; Flynn, M.J.; Gallagher, M.W.; Harrison, R.M.; James, L.; et al. Size distribution, mixing state and source apportionment of black carbon aerosol in London during wintertime. *Atmos. Chem. Phys.* **2014**, *14*, 10061–10084. [[CrossRef](#)]
24. Gong, X.D.; Zhang, C.; Chen, H.; Nizkorodov, S.A.; Chen, J.M.; Yang, X. Size distribution and mixing state of black carbon particles during a heavy air pollution episode in Shanghai. *Atmos. Chem. Phys.* **2016**, *16*, 5399–5411. [[CrossRef](#)]

25. Zhang, Y.J.; Tang, L.L.; Wang, Z.; Yu, H.X.; Sun, Y.L.; Liu, D.; Qin, W.; Canonaco, F.; Prévôt, A.S.H.; Zhang, H.L.; et al. Insights into characteristics, sources, and evolution of submicron aerosols during harvest seasons in the Yangtze River delta region, China. *Atmos. Chem. Phys.* **2015**, *15*, 1331–1349. [[CrossRef](#)]
26. Zhang, Y.; Tang, L.L.; Yu, H.; Wang, Z.; Sun, Y.; Qin, W.; Chen, W.; Chen, C.; Ding, A.; Wu, J.; et al. Chemical composition, sources and evolution processes of aerosol at an urban site in Yangtze River Delta, China during wintertime. *Atmos. Environ.* **2015**, *123*, 339–349. [[CrossRef](#)]
27. Ng, N.L.; Herndon, S.C.; Trimborn, A.; Canagaratna, M.R.; Croteau, P.L.; Onasch, T.B.; Sueper, D.; Worsnop, D.R.; Zhang, Q.; Sun, Y.L.; et al. An aerosol chemical speciation monitor (ACSM) for routine monitoring of the composition and mass concentrations of ambient aerosol. *Aerosol Sci. Technol.* **2011**, *45*, 770–784. [[CrossRef](#)]
28. Sun, Y.L.; Wang, Z.F.; Dong, H.B.; Yang, T.; Li, J.; Pan, X.L.; Chen, P.; Jayne, J.T. Characterization of summer organic and inorganic aerosols in Beijing, China with an aerosol chemical speciation monitor. *Atmos. Environ.* **2012**, *51*, 250–259. [[CrossRef](#)]
29. Jayne, J.T.; Leard, D.C.; Zhang, X.; Davidovits, P.; Smith, K.A.; Kolb, C.E.; Worsnop, D.R. Development of an aerosol mass spectrometer for size and composition analysis of submicron particles. *Aerosol Sci. Technol.* **2000**, *33*, 49–70. [[CrossRef](#)]
30. Zhang, Q.; Jimenez, J.L.; Canagaratna, M.R.; Ulbrich, I.M.; Ng, N.L.; Worsnop, D.R.; Sun, Y. Understanding atmospheric organic aerosols via factor analysis of aerosol mass spectrometry: A review. *Anal. Bioanal. Chem.* **2011**, *401*, 3045–3067. [[CrossRef](#)]
31. Paatero, P.; Tapper, U. Positive matrix factorization: A non-negative factor model with optimal utilization of error estimates of data values. *Environmetrics* **1994**, *5*, 111–126. [[CrossRef](#)]
32. Huang, X.F.; Sun, T.L.; Zeng, L.W.; Guang, H.Y.; Sheng, J.L. Black carbon aerosol characterization in a coastal city in South China using a single particle soot photometer. *Atmos. Environ.* **2012**, *51*, 21–28. [[CrossRef](#)]
33. Laborde, M.; Crippa, M.; Tritscher, T.; Jurányi, Z.; Decarlo, P.F.; Temime-Roussel, B.; Marchand, N.; Eckhardt, S.; Stohl, A.; Baltensperger, U.; et al. Black carbon physical properties and mixing state in the European megacity Paris. *Atmos. Chem. Phys.* **2013**, *13*, 5831–5856. [[CrossRef](#)]
34. Crippa, M.; Canonaco, F.; Lanz, V.A.; Äijälä, M.; Allan, J.D.; Carbone, S.; Capes, G.; Ceburnis, D.; Dall'Osto, M.; Day, D.A.; et al. Organic aerosol components derived from 25 AMS data sets across Europe using a consistent ME-2 based source apportionment approach. *Atmos. Chem. Phys.* **2014**, *14*, 6159–6176. [[CrossRef](#)]
35. Shiraiwa, M.; Kondo, Y.; Moteki, N.; Takegawa, N.; Miyazaki, Y.; Blake, D.R. Evolution of mixing state of black carbon in polluted air from Tokyo. *Geophys. Res. Lett.* **2007**, *34*, L16803. [[CrossRef](#)]
36. Shiraiwa, M.; Kondo, Y.; Moteki, N.; Takegawa, N.; Sahu, L.; Takami, A.; Hatakeyama, S.; Yonemura, S.; Blake, D.R. Radiative impact of mixing state of black carbon aerosol in Asian outflow. *J. Geophys. Res.* **2008**, *113*, D24210. [[CrossRef](#)]
37. Metcalf, A.R.; Craven, J.S.; Ensberg, J.J.; Brioude, J.; Angevine, W.; Sorooshian, A.; Hatakeyama, S.; Yonemura, S.; Blake, D.R. Black carbon aerosol over the Los Angeles basin during CalNex. *J. Geophys. Res.* **2012**, *117*, D00V13. [[CrossRef](#)]
38. Zhang, G.; Bi, X.; He, J.; Chen, D.; Chan, L.Y.; Xie, G.; Wang, X.; Sheng, G.; Fu, J.; Zhou, Z. Variation of secondary coatings associated with elemental carbon by single particle analysis. *Atmos. Environ.* **2014**, *92*, 162–170. [[CrossRef](#)]
39. Wang, Q.Y.; Huang, R.J.; Zhao, Z.Z.; Zhang, N.N.; Wang, Y.C.; Ni, H.Y.; Tie, X.; Han, Y.; Zhuang, M.; Wang, M.; et al. Size distribution and mixing state of refractory black carbon aerosol from a coastal city in South China. *Atmos. Res.* **2016**, *181*, 163–171. [[CrossRef](#)]
40. Drewnick, F.; Hings, S.S.; Curtius, J.; Eerdekens, G.; Williams, J. Measurement of fine particulate and gas-phase species during the New Year's fireworks 2005 in Mainz, Germany. *Atmos. Environ.* **2006**, *40*, 4316–4327. [[CrossRef](#)]
41. Jiang, Q.; Sun, Y.L.; Wang, Z.; Yin, Y. Aerosol composition and sources during the Chinese Spring Festival: Fireworks, secondary aerosol, and holiday effects. *Atmos. Chem. Phys.* **2015**, *15*, 6023–6034. [[CrossRef](#)]
42. Zhang, Y.; Tang, L.; Sun, Y.; Favez, O.; Canonaco, F.; Albinet, A.; Couvidat, F.; Liu, D.; Jayne, J.T.; Wang, Z.; et al. Limited formation of isoprene epoxydiols-derived secondary organic aerosol under NO_x-rich environments in Eastern China. *Geophys. Res. Lett.* **2017**, *44*, 2035–2043. [[CrossRef](#)]

43. Zhang, Y.; Tang, L.; Croteau, P.L.; Favez, O.; Sun, Y.; Canagaratna, M.R.; Wang, Z.; Couvidat, F.; Albinet, A.; Zhang, H.; et al. Field characterization of the PM_{2.5} aerosol chemical speciation monitor: Insights into the composition, sources, and processes of fine particles in eastern China. *Atmos. Chem. Phys.* **2017**, *17*, 14501–14517. [[CrossRef](#)]
44. Xu, J.; Zhang, Q.; Chen, M.; Ge, X.; Ren, J.; Qin, D. Chemical composition, sources, and processes of urban aerosols during summertime in northwest China: Insights from high-resolution aerosol mass spectrometry. *Atmos. Chem. Phys.* **2014**, *14*, 12593–12611. [[CrossRef](#)]



© 2020 by the authors. Licensee MDPI, Basel, Switzerland. This article is an open access article distributed under the terms and conditions of the Creative Commons Attribution (CC BY) license (<http://creativecommons.org/licenses/by/4.0/>).